

Faculty Scholarship

2-14-2023

Minimal Auxiliary Basis Set Approach for the Electronic Excitation Spectra of Organic Molecules

Zehao Zhou

Case Western Reserve University, zehao.zhou@case.edu

Shane M. Parker

Case Western Reserve University, shane.parker@case.edu

Author(s) ORCID Identifier:

[Zehao Zhou](#)

[Shane M. Parker](#)

Follow this and additional works at: <https://commons.case.edu/facultyworks>

Part of the [Computational Chemistry Commons](#), and the [Physical Chemistry Commons](#)
Commons

Network Recommended Citation

Zhou, Zehao and Parker, Shane M., "Minimal Auxiliary Basis Set Approach for the Electronic Excitation Spectra of Organic Molecules" (2023). *Faculty Scholarship*. 71.

<https://commons.case.edu/facultyworks/71>

This Article is brought to you for free and open access by Scholarly Commons @ Case Western Reserve University. It has been accepted for inclusion in Faculty Scholarship by an authorized administrator of Scholarly Commons @ Case Western Reserve University. For more information, please contact digitalcommons@case.edu.

CWRU authors have made this work freely available. [Please tell us](#) how this access has benefited or impacted you!

Minimal auxiliary basis set approach for the electronic excitation spectra of organic molecules

Zehao Zhou,[†] Fabio Della Sala,^{‡,¶} and Shane M. Parker^{*,†}

[†]*Department of Chemistry, Case Western Reserve University, 10900 Euclid Ave, Cleveland, OH 44106, USA*

[‡]*Center for Biomolecular Nanotechnologies, Istituto Italiano di Tecnologia, Via Barsanti 14, 73010 Arnesano (LE), Italy*

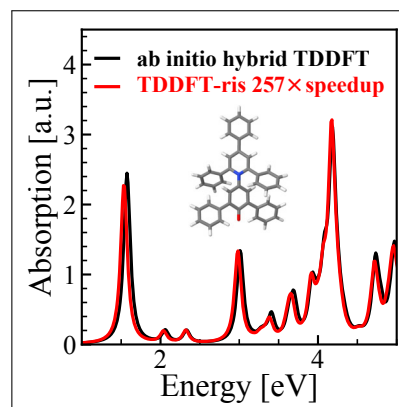
[¶]*Institute for Microelectronics and Microsystems (CNR-IMM), Via Monteroni, Campus Unisalento, 73100 Lecce, Italy*

E-mail: shane.parker@case.edu

Abstract

We report a minimal auxiliary basis model for time-dependent density functional theory (TDDFT) with hybrid density functionals that can accurately reproduce excitation energies and absorption spectra from TDDFT while reducing cost by about two to three orders of magnitude. Our method, dubbed TDDFT-*ris*, employs the resolution-of-the-identity technique with just one *s*-type auxiliary basis function per atom for the linear response operator, where the Gaussian exponents are parametrized across the periodic table using tabulated atomic radii with a single global scaling factor. By tuning on a small test set, we determine a single functional-independent scale factor that balances errors in excitation energies and absorption spectra. Benchmarked on organic molecules and compared to standard TDDFT, TDDFT-*ris* has an average energy error of only 0.06 eV, and yields absorption spectra in close agreement with TDDFT. Thus, TDDFT-*ris* enables simulation of realistic absorption spectra in large molecules that would be inaccessible from standard TDDFT.

TOC Graphic



The prediction of optical properties and the simulation of photochemical processes are central goals in chemical physics, and thus accurate and efficient computational methods are urgently needed.¹⁻⁴ Compared to other state-of-the-art excited-state electronic structure methods, time dependent density functional theory (TDDFT)^{5,6} has among the most favorable accuracy-to-cost ratio.⁷⁻⁹ In the past few decades, different methods have been developed in order to reduce the computational cost.¹⁰⁻¹⁷ One of the most important method is the resolution-of-the-identity (RI) approximation of two electron repulsion integrals (ERI),¹⁸⁻²⁶ also known as density-fitting. However, routine TDDFT simulations of ultraviolet-visible (UV-vis) spectra are still typically limited to systems with a few hundred atoms and a few thousand basis functions because of their computational cost. More specifically, common implementations of TDDFT scale with $O(N^2)$ to $O(N^3)$ where N is a measure of system size. When computing a full spectral window (i.e., simulating the UV-vis absorption spectrum between two user-chosen excitation wavelengths), the scaling depends on the algorithm: algorithms based on computing eigenvalues of the Casida equation scale with the density of states⁵ while algorithms based on real time TDDFT²⁷ or the complex polarization propagator^{28,29} scale with the width and density of the spectral window.³⁰⁻³² Thus, methods to further dramatically reduce the computational cost of TDDFT are key to unlocking first-principles simulations of excited-state properties and spectra for large systems such as nanoparticles and photocatalysts.

One common strategy for avoiding the high computational cost needed to simulate absorption spectra is to use a semiempirical model rather than a first-principles method, because semiempirical models are often several orders of magnitude less expensive than first-principles methods.³³ Three classes of semiempirical models have been proposed for simulating optical spectra in recent decades. In the first class, molecular mechanics force fields were extended to contain frequency-dependent polarization, which allows for the definition of absorption spectra through the imaginary part of the dynamic polarizability.³⁴⁻³⁹

In the second class, both the ground state prob-

lem and the excited-state problem are replaced with semiempirical quantum mechanical treatments. That is, excited states are described as a semiempirical linear response from a semiempirical ground state. Examples of the fully semiempirical models include the semiempirical configuration interaction (CI) models,^{33,40} time-dependent density functional tight-binding (TD-DFTB),⁴¹ and tight-binding based simplified Tamm-Dancoff Approximation (sTDA-xTB).⁴²

The final class uses the first-principles Kohn-Sham (KS) ground state and only introduces approximations to the linear response matrix, i.e., a semiempirical linear response is performed on top of a first-principles ground state. Examples of this class include the simplified Tamm-Dancoff (sTDA) and simplified TDDFT (sTDDFT) models,^{43,44} the TDDFT plus tight-binding (TDDFT+TB) model,⁴⁵ and the simplified GW (sGW) and simplified Bethe-Salpeter equation (sBSE) models.⁴⁶ More recently, a minimal auxiliary basis model for TDDFT (TDDFT-as) was proposed for semilocal density functionals in which the linear response kernel is approximated using RI where the fitting basis for each atom includes only one s -type Gaussian function.⁴⁷ TDDFT-as was applied to silver nanoparticles where an average error of only 12 meV was found. Such error is one order of magnitude smaller than previous semiempirical linear response models that use first-principles ground states. Optimized auxiliary basis-set approaches for TDDFT have been also recently investigated.^{48,49}

Here, we introduce the TDDFT-ris model, a minimal auxiliary basis model for hybrid density functionals parametrized across the entire periodic table. In this Letter, we focus on global hybrid density functionals because these have been shown to perform better than semilocal ones for computing excited states of organic molecules.^{9,50} We will show that TDDFT-ris has a root-mean-square-error (RMSE) relative to TDDFT of 0.06 eV, much lower than the corresponding RMSE of sTDDFT (0.24 eV), and below the typical error of hybrid TDDFT compared to experimental values (about 0.2-0.3 eV).^{9,50}

Within linear response TDDFT, excitation energies are obtained by solving the symplectic eigen-

value equation

$$\begin{pmatrix} \mathbf{A} & \mathbf{B} \\ \mathbf{B} & \mathbf{A} \end{pmatrix} \begin{pmatrix} \mathbf{X} \\ \mathbf{Y} \end{pmatrix} = \begin{pmatrix} \mathbf{1} & \mathbf{0} \\ \mathbf{0} & -\mathbf{1} \end{pmatrix} \begin{pmatrix} \mathbf{X} \\ \mathbf{Y} \end{pmatrix} \boldsymbol{\Omega}, \quad (1)$$

where

$$(A+B)_{ia,jb} = (\varepsilon_a - \varepsilon_i) \delta_{ab} \delta_{ij} + 2(ia|jb) + 2f_{iajb}^{\text{xc}} + c_x[(ib|ja) + (ij|ab)], \quad (2a)$$

$$(A-B)_{ia,jb} = (\varepsilon_a - \varepsilon_i) \delta_{ab} \delta_{ij} + c_x[(ib|ja) - (ij|ab)], \quad (2b)$$

ε_p is the KS eigenvalue associated with KS orbital ϕ_p , f_{iajb}^{xc} is a matrix element of the semilocal exchange-correlation (XC) kernel, $(pq|rs)$ is a matrix element of the four-center two-electron repulsion integral, and c_x is the fraction of Hartree-Fock exchange (HFX). In Eq. (2), labels i, j refer to occupied molecular orbitals (MOs) while a, b refer to virtual MOs.

To arrive at the TDDFT-ris model, we follow the same basic structure as sTDDFT, TDDFT+TB and TDDFT-as: the semilocal XC kernel in Eq. (2) is neglected and the expensive ERIs are approximated with a monopole-like expansion. In TDDFT-ris, the ERIs are approximated using the resolution-of-the-identity technique,

$$(pq|rs) \approx \sum_{AB} (pq|A)(A|B)^{-1}(B|rs), \quad (3)$$

where $(A|B)$ and $(pq|A)$ are two-center and three-center two-electron repulsion integrals, respectively, A,B label atoms and p, q, r, s label generic MOs.⁵¹ Eq. (3) is also employed in TDDFT-as, but only for the Coulomb contribution, whereas in TDDFT-ris this is extended to the HFX. By contrast, in sTDDFT,⁴⁴ ERIs are approximated using

$$(pq|rs) \approx \sum_{AB} Q_{pq}^A \gamma_{AB} Q_{rs}^B, \quad (4)$$

where Q_{pq}^A is the Löwdin charge density matrix on atom A , and γ_{AB} is an effective repulsion between atoms A and B .

The key feature of TDDFT-ris is that just one s -type Gaussian function is used per atom as the auxiliary basis set in Eq. (3), whereas typical auxiliary basis sets include 10-100 functions per atom.⁵² For the Gaussian exponent for atom A , α_A , we propose

to use

$$\alpha_A = \frac{\theta}{R_A^2}, \quad (5)$$

where R_A is the atomic radius for atom A and θ is a yet-to-be-determined global factor. This ansatz originates from observations that 1) the exponent can be related to the square of the Hubbard parameter which is twice the hardness η_A (i.e., $\alpha_A \propto \eta_A^2$)^{41,47,53-55} and 2) the hardness is inversely proportional to the atomic radius (i.e., $\eta_A \propto \frac{1}{R_A}$).⁵⁶ We use semiempirically determined atomic radii proposed by Ghosh et al.⁵⁷ The ansatz Eq. (5) is equivalent to choosing the exponents such that the most probable radii for each element are proportional to the tabulated atomic radii. The benefits of this ansatz are that TDDFT-ris can be defined for all 103 elements with a tabulated atomic radius and there is only a single global parameter, θ , that needs to be optimized. In addition, TDDFT-ris retains the monopole-like form for the ERIs and therefore will lead to cost reductions of two or three orders of magnitude relative to standard TDDFT.

First, we examine the performance of the TDDFT-ris approximation on the π - π^* excitation of ethene, the simplest model for an electronic excitation in an organic molecule. The first singlet π - π^* excitation energy, Ω_s , of ethene can be approximated as

$$\Omega_s \approx \Omega_s^{\text{TDA}} = (\varepsilon_L - \varepsilon_H) + \mathcal{K} + \mathcal{J} \quad (6)$$

with

$$\mathcal{K} = K + F^{\text{xc}} \quad (7a)$$

$$\mathcal{J} = -c_x J \quad (7b)$$

where H denotes the highest-occupied molecular orbital, L denotes the lowest unoccupied molecular orbital, $K = (HL|HL)$, $J = (HH|LL)$, and F^{xc} is the c_x dependent contribution from the XC kernel. For concreteness, we consider the Perdew-Burke-Ernzerhof (PBE) hybrid density functional⁵⁸ with a variable fraction of HFX. Eq. 6 corresponds to the TDA⁵⁹ and is valid when the orbital energy gap is much larger than the kernel contribution, which is true for ethene.

We then apply the TDDFT-ris approximation to

Eq. (6), such that

$$\Omega_s^\alpha = (\varepsilon_L - \varepsilon_H) + \mathcal{K}^\alpha + \mathcal{J}^\alpha \quad (8)$$

with

$$\mathcal{K}^\alpha = K^\alpha \quad (9a)$$

$$\mathcal{J}^\alpha = -c_x J^\alpha, \quad (9b)$$

where the superscript, α , signifies approximating the term using Eq. (3) with the same Gaussian exponent α for each atom, i.e., assuming carbon and hydrogen share the same exponent. Comparing Eq. (7a) and Eq. (9a), we see that our ansatz anticipates error cancellation between K and the semilocal XC kernel, as discussed in Ref. 47.

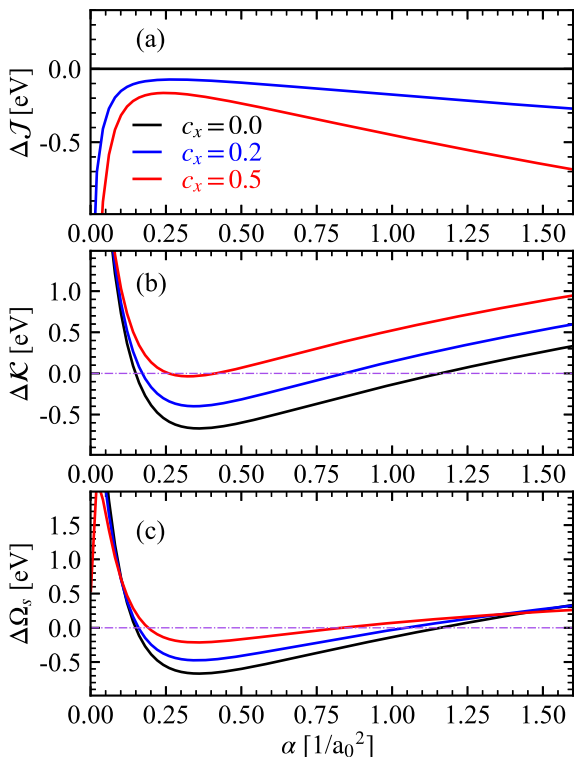


Figure 1: Errors in the (a) HFX integral, $\Delta\mathcal{J}$, (b) Coulomb and XC kernel contributions, $\Delta\mathcal{K}$, and (c) excitation energies, $\Delta\Omega_s$, as a function of the auxiliary basis exponent, α , for ethene with different fractions of the PBE0 HFX (c_x).

In Fig. 1 we report the error in the TDDFT-ris approximation to \mathcal{K} , \mathcal{J} , and Ω_s for several different values of c_x . For each of these quantity, we define $\Delta M = M - M^\alpha$. Because the orbital eigenvalues are not approximated in TDDFT-ris, the er-

ror in the excitation energy is simply

$$\Delta\Omega_s = \Delta\mathcal{K} + \Delta\mathcal{J}. \quad (10)$$

In Fig. 1a, we see that \mathcal{J}^α consistently overestimates \mathcal{J} ($\Delta\mathcal{J} < 0$), as expected from a truncated auxiliary basis, and the overestimation increases with increasing c_x . However, there is a small region of about $0.15\text{-}0.20/a_0^2$ (with a_0 the Bohr radius) in which $\Delta\mathcal{J}$ is minimized for all considered values of c_x . By contrast, we see in Fig. 1b that $\Delta\mathcal{K}$ is neither consistently negative nor positive, because the approximations in \mathcal{K}^α are counteracting: neglecting F^{xc} increases \mathcal{K}^α ($F^{\text{xc}} < 0$) while the RI approximation underestimates the repulsion energy which decreases \mathcal{K}^α . Finally, in Fig. 1c, we see two regions where $\Delta\Omega_s$ is small: one near $\alpha = 0.18/a_0^2$ and one near $\alpha = 1.0/a_0^2$. However, by inspecting $\Delta\mathcal{J}$ and $\Delta\mathcal{K}$, we see that, for $c_x > 0$, the minimum with $\alpha = 1.0/a_0^2$ relies on large and fortuitous error cancellation between \mathcal{J}^α and \mathcal{K}^α , whereas the individual errors at the minimum near $\alpha = 0.18/a_0^2$ are much smaller. Thus, we conclude that the TDDFT-ris model can reproduce excitation energies in organic molecules with a properly chosen exponent and that more diffuse (smaller α) exponents are likely to provide more robust error cancellation.

With this encouraging result, we turn to determining the global scaling factor, θ , by minimizing the error in both excitation energies and spectra across a small tuning set. Our tuning set, TUNE20, consists of 20 small-to-large organic molecules and includes natural compounds, biomolecules, organic dyes, chemical probes, and drugs. See Fig. S1 in the Supporting Information for the composition of TUNE20. We evaluated TUNE20 using three hybrid density functionals with different amounts of HFX: TPSSH with $c_x = 0.1$,⁶⁰ PBE0 with $c_x = 0.25$,⁵⁸ and BH&H-LYP with $c_x = 0.5$.⁶¹ All tuning calculations used the def2-SVP basis set.⁶² We considered two complementary error metrics for the performance of TDDFT-ris, i) the RMSE in the lowest 20 excitation energies, E_{ene} , and ii) the normalized percentage error in the absorption spectrum, E_{spe} (see Computational Details for the precise definition).

The average energy error, E_{ene} , and the average spectral error, E_{spe} , across the TUNE20 set are

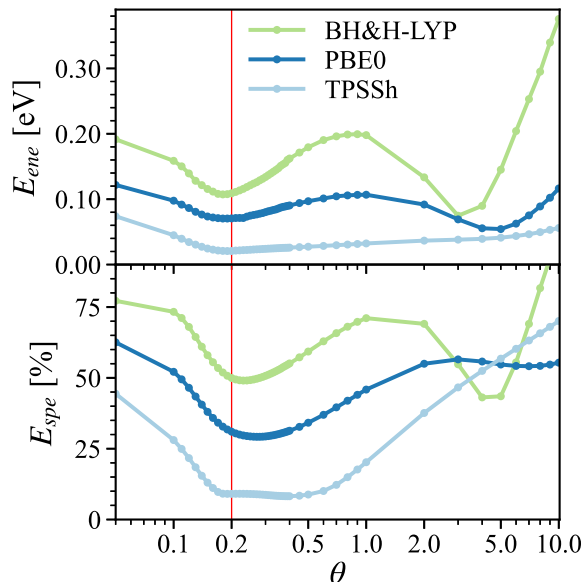


Figure 2: The average E_{ene} and E_{spe} for TUNE20 of TDDFT-ris versus the global scaling factor θ (in log10 scale), for the TPSSh, PBE0 and BH&H-LYP density functionals. The vertical red line indicates the chosen global value of $\theta = 0.2$.

shown in Fig. 2 as a function of the global scaling factor, θ . Similar to the ethene example, local minima were found in two distinct regions, one region centered around $\theta = 0.2$ and the other at $\theta \in [3, 5]$. In the region near $\theta = 0.2$, E_{ene} and E_{spe} exhibit local minima for all three functionals. Although we see a slight increase in E_{ene} and E_{spe} as the percentage of HFX increases in each functional, the location of the minimum is relatively insensitive to the XC functional or to the metric. On the other hand, in the $\theta \in [3, 5]$ region, we see starkly different behavior with different XC functionals, indicating that the fortuitous error cancellation for large exponents already seen in Fig. 1 is highly sensitive to the XC functional. Furthermore, E_{spe} grows with larger θ , except for the highest c_x , and the transition density becomes increasingly localized around the atomic cores, which is physically incorrect. Thus we use the region near $\theta = 0.2$ to determine the global scaling factor. In particular, we see that for E_{ene} , a θ value slightly less than 0.2 is preferred, whereas for E_{spe} , a θ value slightly larger than 0.2 is preferred. Therefore, we choose $\theta = 0.2$ as a compromise between energy and spectral errors. Detailed results for all systems are reported in Fig. S2 of the Supporting Informa-

tion.

Before considering the performance of TDDFT-ris for excitation energies and spectra, we first confirm that the choice $\theta = 0.2$ produces near-optimal exponents for a simple polycyclic aromatic hydrocarbon, naphthalene, by computing E_{ene} while individually tuning the exponents on hydrogen, α_H , and carbon, α_C . We focus on the PBE0 density functional because of its excellent performance in organic systems⁶³ and use the def2-TZVP basis set.

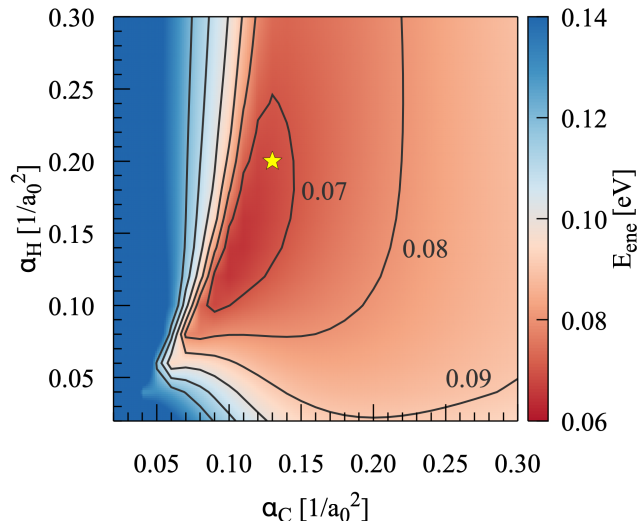


Figure 3: Two-dimensional scan of E_{ene} (in eV) as a function of α_C and α_H for naphthalene for the PBE0 functional and def2-TZVP basis set. The star at $(\alpha_C, \alpha_H) = (0.13/a_0^2, 0.2/a_0^2)$ shows the exponents determined using Eq. (5) with $\theta = 0.2$.

Fig. 3 shows the resulting two-dimensional scan of the exponents, from which we can see a well-defined minimum where $\alpha_C \in [0.09 - 0.14]/a_0^2$ and $\alpha_H \in [0.1 - 0.22]/a_0^2$ with E_{ene} less than 0.07 eV. The α_C exponent is more defined than α_H as the transitions considered are mostly localized on carbon atoms. For comparison, using $\theta = 0.2$, we find exponents of $\alpha_C = 0.13/a_0^2$ and $\alpha_H = 0.20/a_0^2$, inside the region with $E_{ene} < 0.07$ eV. The results are nearly identical using def2-SVP (see Fig. S3 in the Supporting Information). We emphasize that naphthalene is *not* included in the TUNE20 set, thus showing that our parametrization recovers the manually optimized exponents for naphthalene.

As a further test of our approach, we can compare the exponent obtained here to the exponent

reported for Ag nanocrystals with TDDFT-as. Using Eq. (5), we obtain $\alpha_{\text{Ag}} = 0.014/a_0^2$, which is significantly smaller than the exponent obtained in Ref. 47, $\alpha_{\text{Ag}} = 0.036/a_0^2$. This large difference is the result of different strategies and systems used to determine the exponents; the exponent in Ref. 47 was hand optimized for silver nanoparticles using a semilocal density functional, whereas Eq. (5) is a global parametrization for hybrid functionals that was tuned against TUNE20, which contains organic molecules and no Ag. Although the change in the exponent is large, it has only a minor effect on the quality of the results. Using our proposed value of α_{Ag} in TDDFT-as with the PBE functional, the E_{ene} in Ref. 47 would only slightly increase from 12 meV to 20 meV.

Next, we evaluate the performance of the TDDFT-*ris* model by computing excitation energies and spectra for an extended test set of 42 organic molecules (EXTEST42, see Fig. S1 in the Supporting Information for a full definition). We compare the results to standard TDDFT as the reference and to sTDDFT, because it is a similarly structured semiempirical model. We note that sTDDFT was parametrized using experimental excitation energies, whereas TDDFT-*ris* was parametrized using TDDFT. All benchmarks and spectra used the PBE0 density functional⁵⁸ and def2-TZVP basis set.⁶²

The E_{ene} and E_{spe} for each molecule in EXTEST42 are shown in Fig. 4. E_{ene} is systematically reduced in TDDFT-*ris* relative to sTDDFT for *all* molecules in EXTEST42. The average E_{ene} across EXTEST42, $\langle E_{ene} \rangle$, is just 0.058 eV with TDDFT-*ris*, compared to 0.24 eV with sTDDFT (see Table 1). For context, $\langle E_{ene} \rangle$ using TDDFT-*ris* is below the expected error of PBE0 (0.2-0.3 eV).^{9,50} Also, the average error of the lowest-lying excited state, $\langle E_{S_1} \rangle$, with TDDFT-*ris* is 0.068 eV, which is similar to the basis set incompleteness error (e.g., S_1 energies in EXTEST42 shift on average by 0.063 eV when going from def2-TZVP to def2-SVP, see Table SI in the Supporting Information). Similarly, the average error in the absorption spectra, $\langle E_{spe} \rangle$, is 28% using TDDFT-*ris*, compared to 59% using sTDDFT (Table 1). However, in contrast to the E_{ene} data, E_{spe} is lower using sTDDFT for three molecules. Finally, in Table 1 we see that the high accuracy of TDDFT-*ris* is unchanged when

considering only the S_1 , whereas the performance of sTDDFT improves slightly. Thus, TDDFT-*ris* has a more stable accuracy across a wider energy-range and outperforms sTDDFT in computing the optical gap, and the absorption spectrum.

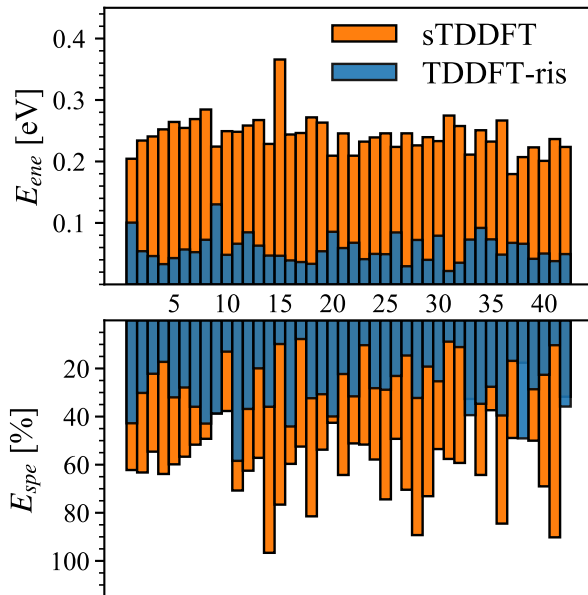


Figure 4: The energy error E_{ene} and spectra error E_{spe} of sTDDFT and TDDFT-*ris* on EXTEST42. Calculations are done with PBE0/def2-TZVP. Molecules are sorted same as Table SI in the Supporting Information.

Table 1: Average energy, spectral and S_1 errors of TDDFT-*ris* and sTDDFT using standard TDDFT as reference. Calculations are done with PBE0/def2-TZVP.

MAE	TDDFT- <i>ris</i>	sTDDFT
$\langle E_{ene} \rangle$ [eV]	0.058	0.24
$\langle E_{spe} \rangle$ [%]	28	59
$\langle E_{S_1} \rangle$ [eV]	0.068	0.19

As a final assessment of the TDDFT-*ris* performance, we show absorption spectra computed for three representative examples in EXTEST42: retinal, a tetraphenyl aza-BODIPY dye investigated in Ref. 64,65 and referred to as BF₂(WS3), and provitamin D₃. The results are shown in Fig. 5. For retinal (Fig. 5a) TDDFT-*ris* correctly reproduces the position and the intensity of all peaks better than sTDDFT does. Including excitations

up to 7 eV, TDDFT-ris has E_{ene} of 0.05 eV and E_{spe} of 23%, while sTDDFT has E_{ene} of 0.23 eV and $E_{spe} = 97\%$. As an example, the lowest energy bright TDDFT peak at 2.92 eV is red shifted by 0.06 eV and the intensity overestimated by 3% using TDDFT-ris, compared to a red shift of 0.21 eV and an underestimated oscillator strength of 17%.

For molecule $\text{BF}_2(\text{WS3})$ (Fig. 5b), we see that TDDFT-ris reproduces the TDDFT absorption spectra almost exactly ($E_{ene} = 0.04$ eV and $E_{spe} = 11\%$) and much better than sTDDFT ($E_{ene} = 0.26$ eV and $E_{spe} = 59\%$).

For provitamin D_3 (Fig. 5c), which is a challenging case, we find $E_{ene} = 0.04$ eV and E_{spe} of 44% with TDDFT-ris, compared to $E_{ene} = 0.24$ eV and $E_{spe} = 60\%$ with sTDDFT. UV-vis spectra with PBE0 for all other molecules are shown in Fig. S4 in Supporting Information.

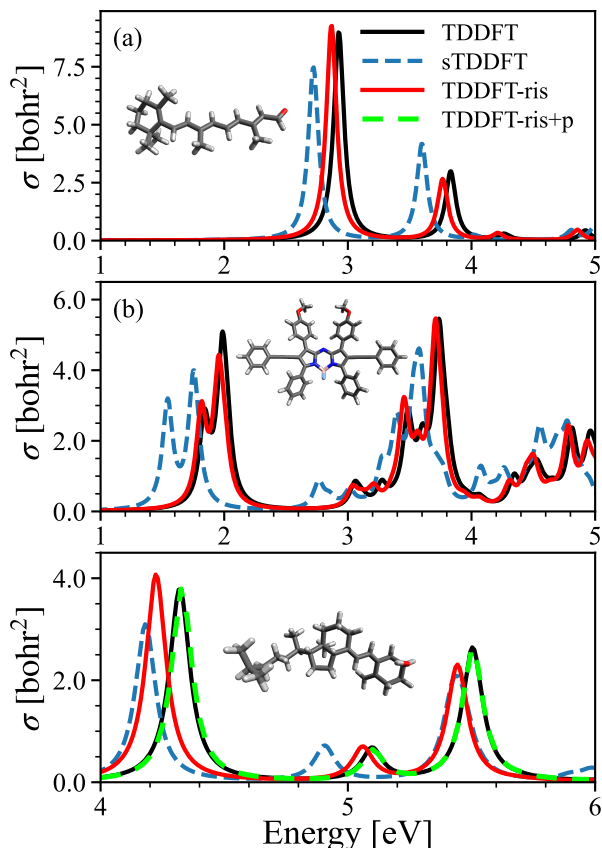


Figure 5: The simulated UV spectra for (a) retinal, 20 states, (b) $\text{BF}_2(\text{WS3})$, 63 states, (c) provitamin D_3 , 20 states. Spectra were calculated with PBE0/def2-TZVP and broadened with a Lorentzian with full-width-at-half-maximum (FWHM) of 0.1 eV.

Table 2: Computation cost comparison of TDDFT, TDDFT-ris and sTDDFT computing 20 excitation energies in retinal with PBE0/def2-TZVP. n_{occ} is the number of occupied MOs, n_{vir} the number of virtual MOs.

	TDDFT	TDDFT-ris	sTDDFT
Total time [s]	16,974	46	8
Coulomb [s]	241	2.9	n/a
HFX [s]	15,104	29.5	n/a
XC [s]	1,642	1.0	n/a
E_{ene} [eV]	0	0.05	0.23
speedup	1	369	2,121
n_{occ}	78	78	56
n_{vir}	741	741	134
CSFs	57,798	57,798	124

A crucial motivation for the TDDFT-ris model is to dramatically reduce the computational cost of standard TDDFT. In Table 2, we collect results from timing the calculation of the lowest 20 states of retinal using standard TDDFT, TDDFT-ris, and sTDDFT. Our pilot implementation of TDDFT-ris uses the RI-J and RI-K engine in Turbomole with a custom auxiliary basis.⁶⁶ We find that TDDFT-ris is 369 times faster than standard TDDFT, reducing the total central processing unit (CPU) time from 4.5 hours to 46 seconds. The largest contribution to the speedup comes the HFX integral, which from 4 hours to 30 second, a factor of 510 speedup. This dramatic speedup in terms of CPU time incurs only a minor error of 0.05 eV.

In Table 2, we can see that sTDDFT (using sTDA as described in the Computational Details) is significantly faster than our current TDDFT-ris implementation, with an overall speedup of 2121 relative to standard TDDFT and a speedup of 6 relative to TDDFT-ris. The superior speed of the sTDDFT is the result of several innovations in the sTDA implementation, including an aggressive truncation of the MO space and the number of configuration state functions (CSFs) considered, a perturbative correction to account for neglected MOs and CSFs, the use of single precision floating point arithmetic, and full diagonalization of the response matrix.^{43,44,67} By contrast, the TDDFT-ris results presented here used no MO

or CSF truncation and used double precision floating point arithmetic with iterative Krylov space eigenvalue solvers.³¹ However, because the ERI approximations in TDDFT-*ris* and sTDDFT have similar structures, these same innovations are fully compatible with TDDFT-*ris*.

In conclusion, we have introduced a minimal auxiliary basis set model for TDDFT, called TDDFT-*ris*, that reproduces hybrid TDDFT excitation energies of organic molecules to within 0.06 eV on average (using PBE0) while reducing computational cost by 2-3 orders of magnitude. The key ingredients of the TDDFT-*ris* model are that 1) the semilocal XC kernel is neglected, and 2) the electron repulsion integrals are approximated with a resolution-of-the-identity using just a single *s*-type Gaussian function per atom in the auxiliary basis. The exponents in the auxiliary basis TDDFT-*ris* were chosen to be proportional to the inverse square of tabulated atomic radii such that TDDFT-*ris* is immediately applicable across the periodic table. Furthermore, we find that the optimal exponents for the auxiliary basis set of the TDDFT-*ris* model are almost independent of the choice of the XC density functional. We attribute the excellent performance of TDDFT-*ris* for both excitation energies and spectra to the explicit description of transition densities using the minimal auxiliary basis. By contrast, tight-binding approaches^{43,45,46} describe transition densities implicitly with Löwdin charge densities, which have numerical as opposed to physical definitions.^{68,69} The TDDFT-*ris* model therefore opens up the possibility of computing accurate absorption spectra and optical properties for organic molecules with many hundreds of atoms using hybrid density functionals that may not be affordable otherwise.

A significant advantage of TDDFT-*ris* is that it uses the standard RI engine for Coulomb and exchange, can therefore be enabled from an existing RI implementation by simply neglecting the XC kernel. Thus, we expect potentially rapid adoption of TDDFT-*ris* in other electronic structure programs. Furthermore, by relying on existing implementations, TDDFT-*ris* could be immediately defined and usable in conjunction with other advanced features such as continuum solvation, range-separated hybrid density functionals, and electric and magnetic linear and nonlinear

properties. In addition, the similarity in structure to sTDDFT means that TDDFT-*ris* can be used as a replacement for sTDDFT. For example, sTDDFT has been used as a preconditioner for Krylov space methods to speed up calculations of TDDFT excitation energies with no loss of accuracy;⁷⁰ we expect TDDFT-*ris* to be an even more effective preconditioner.

Another advantage of TDDFT-*ris* is that the strong physical motivation underlying TDDFT-*ris* means it will be more systematically improvable than models based purely on tight binding. For example, a semiempirical grid-free XC kernel correction for TDDFT-*ris* would be expected to increase the accuracy of the model. This would be especially beneficial for triplet excitations, which are expected to poorly described in TDDFT-*ris* without an explicit contribution from the magnetic XC kernel.⁴⁵ Another example is that the systematic failure of TDDFT-*ris* and sTDDFT to describe excitations dominated by transitions between high angular momentum orbitals on the same atom, such as d-d transitions in metal complexes or p_x-p_y transitions in organic molecules, could be cured. In such molecules, these highly localized excitations could be recovered by expanding the auxiliary basis on selected atoms with important excitations.

We envision an extendable hierarchy of TDDFT-*ris* methods that can further improve the accuracy in specific systems. As an illustration, we considered an extension of TDDFT-*ris* to include one *p* shell for non-hydrogen atoms while naively using the same exponent used for the *s* function (temporarily referred to as TDDFT-*ris*+*p*). We found that TDDFT-*ris*+*p* further reduces $\langle E_{ene} \rangle$ across EXTEST42 to 0.04 eV, an additional 34% reduction. As an example, we can see in Fig. 5c that with TDDFT-*ris*+*p* the absorption spectrum of provitamin D₃ is nearly indistinguishable from the absorption spectrum computed with standard TDDFT. This extension would also cure the artificial decoupling of σ and π^* orbitals present in linear response tight binding methods like TD-DFTB.⁷¹ A complementary strategy to improve TDDFT-*ris* would be to tune the model for specific systems, either by adjusting θ or by adjusting the exponents for each atom independently to account for different environments. Such environment-

dependent exponents could be determined from information available in the Kohn-Sham ground state or could potentially be machine-learned so that the optimal auxiliary basis set exponent can be automatically determined for each specific system.

Computational details

For all DFT and TDDFT calculations, we used the Turbomole³² 7.5 program package with the RI-J technique for the Coulomb term.^{20,72} All ground state geometries of TUNE20 and EXTEST42 were optimized using TPSS⁷³/D3BJ^{74,75}/def2-SVP⁶² in vacuum. Instructions and an automated script are available⁷⁶ to enable TDDFT-ris calculations starting in TURBOMOLE 7.7.

For the sTDDFT calculations on EXTEST42, we use the sTDA package v1.6.2⁶⁷ with $c_x = 0.25$ for PBE0, an energy threshold (spectra window) of 9 eV, and focused on the lowest 20 eigenvectors (-ax 0.25 -e 9 -rpa -vectm 20), leaving other options as default.

The RMSE metric for excitation energies is defined as

$$E_{ene} = \left(\frac{\sum_{i=1}^N (\Omega_i^{\text{ref}} - \Omega_{j(i)})^2}{N} \right)^{1/2}, \quad (11)$$

where Ω_i^{ref} is the i -th excitation energy computed using TDDFT, $\Omega_{j(i)}$ is the corresponding excitation energy from the approximate method, $N = 20$ is the number of excited states considered and the function $j(i)$ ⁴⁷ associates the excited state i of the standard TDDFT calculation with the excited state j in the approximate calculation, thereby avoiding state flipping in the comparison of excitation energies.

The metric for the error in the spectra is defined as

$$E_{spe} = \frac{\int_0^{\omega_{\text{max}}} |\sigma^{\text{ref}}(\omega) - \sigma(\omega)| d\omega}{\int_0^{\omega_{\text{max}}} \sigma^{\text{ref}}(\omega) d\omega}, \quad (12)$$

where ω_{max} is the energy of the highest state considered, $\sigma^{\text{ref}}(\omega)$ is the broadened spectrum from TDDFT and $\sigma(\omega)$ is the broadened spectrum from the approximate method. We used a Lorentzian broadening factor with FWHM = 0.2 eV. For both

sTDDFT and TDDFT-ris we compute all excitation energies up to 5 eV or 20 states, whichever is greater.

The calculations for retinal in Table 2 were performed on a single core of Intel(R) Xeon(R) Gold 6230 CPU @2.10 GHz. For both TDDFT and TDDFT-ris, convergence criteria set as residual norm $\leq 10^{-5}$; for sTDDFT we used energy threshold as 6.3 eV to compute 20 states (-ax 0.25 -e 6.3 -rpa -vectm 20).

All the calculation data in this work is available on OSF⁷⁷ under the MIT License. The plugin called *escfrisprep* to invoke TDDFT-ris and TDDFT-ris+p method in TURBOMOLE Version 7.7 is available on Github⁷⁶ under the MIT license.

Acknowledgement This work was supported by a startup fund from Case Western Reserve University. This work made use of the High Performance Computing Resource in the Core Facility for Advanced Research Computing at Case Western Reserve University.

Supporting Information Available

The following files are available free of charge. Supporting information: detailed information about the TUNE20 and EXTEST42 sets, θ vs error plots for each molecule in TUNE20, S_1 energies and errors for all systems with different methods, additional two-dimensional scans of the exponents for naphthalene, and UV-vis absorption spectra with PBE0 functional for all systems.

References

- (1) Ferré, N.; Filatov, M.; Huix-Rotllant, M.; Adamo, C. *Density-functional methods for excited states*; Springer, 2016; Vol. 368.
- (2) Improta, R.; Santoro, F.; Blancafort, L. Quantum Mechanical Studies on the Photo-physics and the Photochemistry of Nucleic Acids and Nucleobases. *Chem. Rev.* **2016**, *116*, 3540–3593, PMID: 26928320.
- (3) Blase, X.; Duchemin, I.; Jacquemin, D.

- The Bethe–Salpeter equation in chemistry: relations with TD-DFT, applications and challenges. *Chem. Soc. Rev.* **2018**, *47*, 1022–1043.
- (4) Mai, S.; González, L. Molecular Photochemistry: Recent Developments in Theory. *Angew. Chem., Int. Ed. Engl.* **2020**, *59*, 16832–16846.
 - (5) Casida, M. E. In *Recent Advances in Density Functional Methods, vol. 1*; Chong, D. P., Ed.; World Scientific: Singapore, 1995; pp 155–192.
 - (6) Ullrich, C. A. *Time-Dependent Density-Functional Theory: Concepts and Applications*; Oxford Graduate Texts; Oxford University Press: Oxford; New York, 2012.
 - (7) Sarkar, R.; Boggio-Pasqua, M.; Loos, P.-F.; Jacquemin, D. Benchmarking TD-DFT and Wave Function Methods for Oscillator Strengths and Excited-State Dipole Moments. *J. Chem. Theory Comput.* **2021**, *17*, 1117–1132.
 - (8) Shao, Y.; Mei, Y.; Sundholm, D.; Kaila, V. R. I. Benchmarking the Performance of Time-Dependent Density Functional Theory Methods on Biochromophores. *J. Chem. Theory Comput.* **2020**, *16*, 587–600.
 - (9) Liang, J.; Feng, X.; Hait, D.; Head-Gordon, M. Revisiting the Performance of Time-Dependent Density Functional Theory for Electronic Excitations: Assessment of 43 Popular and Recently Developed Functionals from Rungs One to Four. *J. Chem. Theory Comput.* **2022**, *18*, 3460–3473.
 - (10) Walker, B.; Saitta, A. M.; Gebauer, R.; Baroni, S. Efficient Approach to Time-Dependent Density-Functional Perturbation Theory for Optical Spectroscopy. *Phys. Rev. Lett.* **2006**, *96*, 113001.
 - (11) Rocca, D.; Gebauer, R.; Saad, Y.; Baroni, S. Turbo charging time-dependent density-functional theory with Lanczos chains. *J. Chem. Phys.* **2008**, *128*, 154105.
 - (12) Wu, F.; Liu, W.; Zhang, Y.; Li, Z. Linear-Scaling Time-Dependent Density Functional Theory Based on the Idea of From Fragments to Molecule. *J. Chem. Theory Comput.* **2011**, *7*, 3643–3660.
 - (13) Zuehlsdorff, T. J.; Hine, N. D. M.; Spencer, J. S.; Harrison, N. M.; Riley, D. J.; Haynes, P. D. Linear-scaling time-dependent density-functional theory in the linear response formalism. *J. Chem. Phys.* **2013**, *139*, 064104.
 - (14) Baseggio, O.; Fronzoni, G.; Stener, M. A new time dependent density functional algorithm for large systems and plasmons in metal clusters. *J. Chem. Phys.* **2015**, *143*, 024106.
 - (15) Brabec, J.; Lin, L.; Shao, M.; Govind, N.; Yang, C.; Saad, Y.; Ng, E. G. Efficient Algorithms for Estimating the Absorption Spectrum within Linear Response TDDFT. *J. Chem. Theory Comput.* **2015**, *11*, 5197.
 - (16) Gao, Y.; Neuhauser, D.; Baer, R.; Rabani, E. Sublinear scaling for time-dependent stochastic density functional theory. *J. Chem. Phys.* **2015**, *142*, 034106.
 - (17) Baseggio, O.; De Vetta, M.; Fronzoni, G.; Stener, M.; Sementa, L.; Fortunelli, A.; Calzolari, A. Photoabsorption of Icosahedral Noble Metal Clusters: An Efficient TDDFT Approach to Large-Scale Systems. *J. Phys. Chem. C* **2016**, *120*, 12773–12782.
 - (18) Baerends, E.; Ellis, D.; Ros, P. Self-consistent molecular Hartree–Fock–Slater calculations I. The computational procedure. *Chem. Phys.* **1973**, *2*, 41.
 - (19) Dunlap, B. I.; Connolly, J. W. D.; Sabin, J. R. On some approximations in applications of $X\alpha$ theory. *J. Chem. Phys.* **1979**, *71*, 3396.
 - (20) Eichkorn, K.; Treutler, O.; Öhm, H.; Häser, M.; Ahlrichs, R. Auxiliary basis sets to approximate Coulomb potentials. *Chem. Phys. Lett.* **1995**, *240*, 283.

- (21) Bauernschmitt, R.; Häser, M.; Treutler, O.; Ahlrichs, R. Calculation of excitation energies within time-dependent density functional theory using auxiliary basis set expansions. *Chem. Phys. Lett.* **1997**, *264*, 573.
- (22) Heinze, H. H.; Görling, A.; Rösch, N. An efficient method for calculating molecular excitation energies by time-dependent density-functional theory. *J. Chem. Phys.* **2000**, *113*, 2088.
- (23) Neese, F.; Olbrich, G. Efficient use of the resolution of the identity approximation in time-dependent density functional calculations with hybrid density functionals. *Chem. Phys. Lett.* **2002**, *362*, 170.
- (24) Pedersen Thomas Bondo,; Aquilante Francesco,; Lindh Roland, Density fitting with auxiliary basis sets from Cholesky decompositions. *Theor. Chem. Acc.* **2009**, *124*, 1.
- (25) Weigend, F.; Kattannek, M.; Ahlrichs, R. Approximated electron repulsion integrals: Cholesky decomposition versus resolution of the identity methods. *J. Chem. Phys.* **2009**, *130*, 164106.
- (26) Stoychev, G. L.; Auer, A. A.; Neese, F. Automatic Generation of Auxiliary Basis Sets. *J. Chem. Theory Comput.* **2017**, *13*, 554.
- (27) Müller, C.; Sharma, M.; Sierka, M. Real-Time Time-Dependent Density Functional Theory Using Density Fitting and the Continuous Fast Multipole Method. *J. Comput. Chem.* **2020**, *41*, 2573–2582.
- (28) Ekström, U.; Norman, P.; Carravetta, V.; Ågren, H. Polarization Propagator for X-Ray Spectra. *Phys. Rev. Lett.* **2006**, *97*, 143001.
- (29) Creutzberg, J.; Hedegård, E. D. Polarizable Embedding Complex Polarization Propagator in Four- and Two-Component Frameworks. *J. Chem. Theory Comput.* **2022**, *18*, 3671–3686.
- (30) Zuehlsdorff, T. J.; Hine, N. D. M.; Spencer, J. S.; Harrison, N. M.; Riley, D. J.; Haynes, P. D. Linear-Scaling Time-Dependent Density-Functional Theory in the Linear Response Formalism. *J. Chem. Phys.* **2013**, *139*, 064104.
- (31) Furche, F.; Krull, B. T.; Nguyen, B. D.; Kwon, J. Accelerating Molecular Property Calculations with Nonorthonormal Krylov Space Methods. *J. Chem. Phys.* **2016**, *144*, 174105.
- (32) Balasubramani, S. G. et al. TURBOMOLE: Modular Program Suite for Ab Initio Quantum-Chemical and Condensed-Matter Simulations. *J. Chem. Phys.* **2020**, *152*, 184107.
- (33) Thiel, W. Semiempirical quantum–chemical methods. *WIREs Comput. Mol. Sci.* **2014**, *4*, 145–157.
- (34) Mayer, A.; Lambin, P.; Åstrand, P.-O. An electrostatic interaction model for frequency-dependent polarizability: methodology and applications to hydrocarbons and fullerenes. *Nanotechnology* **2008**, *19*, 025203.
- (35) Jensen, L.; Åstrand, P.-O.; Mikkelsen, K. V. Molecular Mechanics Interaction Models for Optical Electronic Properties. *J. Comput. Theor. Nanosci.* **2009**, *6*, 270–291.
- (36) Smalø, H. S.; Åstrand, P.-O.; Mayer, A. Combined nonmetallic electronegativity equalisation and point–dipole interaction model for the frequency-dependent polarizability. *Mol. Phys.* **2013**, *111*, 1470–1481.
- (37) Chen, X.; Moore, J. E.; Zekarias, M.; Jensen, L. Atomistic electrostatics simulations of bare and ligand-coated nanoparticles in the quantum size regime. *Nat. Commun.* **2015**, *6*, 1–8.
- (38) Cheng, Y.; Verstraelen, T. A new framework for frequency-dependent polarizable force fields. *J. Chem. Phys.* **2022**, *157*, 124106.
- (39) Giovannini, T.; Bonatti, L.; Lafiosca, P.; Nicoli, L.; Castagnola, M.; Illobre, P. G.;

- Corni, S.; Cappelli, C. Do We Really Need Quantum Mechanics to Describe Plasmonic Properties of Metal Nanostructures? *ACS Photonics* **2022**, *9*, 3025–3034.
- (40) Giesecking, R. L. M. A New Release of MOPAC Incorporating the INDO/S Semiempirical Model with CI Excited States. *J. Comput. Chem.* **2021**, *42*, 365–378.
- (41) Niehaus, T. A.; Suhai, S.; Della Sala, F.; Lugli, P.; Elstner, M.; Seifert, G.; Frauenheim, T. Tight-Binding Approach to Time-Dependent Density-Functional Response Theory. *Phys. Rev. B* **2001**, *63*, 085108.
- (42) Grimme, S.; Bannwarth, C. Ultra-Fast Computation of Electronic Spectra for Large Systems by Tight-Binding Based Simplified Tamm-Dancoff Approximation (sTDA-xTB). *J. Chem. Phys.* **2016**, *145*, 054103.
- (43) Grimme, S. A Simplified Tamm-Dancoff Density Functional Approach for the Electronic Excitation Spectra of Very Large Molecules. *J. Chem. Phys.* **2013**, *138*, 244104.
- (44) Bannwarth, C.; Grimme, S. A Simplified Time-Dependent Density Functional Theory Approach for Electronic Ultraviolet and Circular Dichroism Spectra of Very Large Molecules. *Comput. Theor. Chem.* **2014**, *1040–1041*, 45–53.
- (45) Rürger, R.; van Lenthe, E.; Heine, T.; Visscher, L. Tight-binding approximations to time-dependent density functional theory — A fast approach for the calculation of electronically excited states. *J. Chem. Phys.* **2016**, *144*, 184103.
- (46) Cho, Y.; Bintrim, S. J.; Berkelbach, T. C. Simplified GW/BSE Approach for Charged and Neutral Excitation Energies of Large Molecules and Nanomaterials. *J. Chem. Theory Comput.* **2022**, *18*, 3438–3446.
- (47) Giannone, G.; Della Sala, F. Minimal Auxiliary Basis Set for Time-Dependent Density Functional Theory and Comparison with Tight-Binding Approximations: Application to Silver Nanoparticles. *J. Chem. Phys.* **2020**, *153*, 084110.
- (48) Medves, M.; Fronzoni, G.; Stener, M. Optimization of density fitting auxiliary Slater-type basis functions for time-dependent density functional theory. *J. Comput. Chem.* **2022**, *43*, 1923–1935.
- (49) Hellmann, L.; Tölle, J.; Niemeyer, N.; Neugebauer, J. Automated Generation of Optimized Auxiliary Basis Sets for Long-Range-Corrected TDDFT Using the Cholesky Decomposition. *J. Chem. Theory Comput.* **2022**, *18*, 2959–2974.
- (50) Jacquemin, D.; Wathelet, V.; Perpète, E. A.; Adamo, C. Extensive TD-DFT Benchmark: Singlet-Excited States of Organic Molecules. *J. Chem. Theory Comput.* **2009**, *5*, 2420–2435.
- (51) Krause, K.; Klopper, W. Implementation of the Bethe-Salpeter Equation in the TURBO-MOLE Program. *J. Comput. Chem.* **2017**, *38*, 383–388.
- (52) Jung, Y.; Sodt, A.; Gill, P. M. W.; Head-Gordon, M. Auxiliary Basis Expansions for Large-Scale Electronic Structure Calculations. *Proc. Natl. Acad. Sci. U.S.A.* **2005**, *102*, 6692–6697.
- (53) York, D. M.; Yang, W. A chemical potential equalization method for molecular simulations. *J. Chem. Phys.* **1996**, *104*, 159–172.
- (54) Chelli, R.; Procacci, P. A transferable polarizable electrostatic force field for molecular mechanics based on the chemical potential equalization principle. *J. Chem. Phys.* **2002**, *117*, 9175–9189.
- (55) Mayer, A. Polarization of metallic carbon nanotubes from a model that includes both net charges and dipoles. *Phys. Rev. B* **2005**, *71*, 235333.
- (56) Ghosh, D. C.; Islam, N. Semiempirical evaluation of the global hardness of the atoms of 103 elements of the periodic table using the most probable radii as their size descriptors.

- Int. J. Quantum Chem.* **2010**, *110*, 1206–1213.
- (57) Ghosh, D. C.; Biswas, R.; Chakraborty, T.; Islam, N.; Rajak, S. K. The Wave Mechanical Evaluation of the Absolute Radii of Atoms. *J. Mol. Struct.(THEOCHEM)* **2008**, *865*, 60–67.
- (58) Perdew, J. P.; Ernzerhof, M.; Burke, K. Rationale for Mixing Exact Exchange with Density Functional Approximations. *J. Chem. Phys.* **1996**, *105*, 9982–9985.
- (59) Hirata, S.; Head-Gordon, M. Time-Dependent Density Functional Theory within the Tamm-Dancoff Approximation. *Chem. Phys. Lett.* **1999**, *314*, 291–299.
- (60) Staroverov, V. N.; Scuseria, G. E.; Tao, J.; Perdew, J. P. Comparative Assessment of a New Nonempirical Density Functional: Molecules and Hydrogen-Bonded Complexes. *J. Chem. Phys.* **2003**, *119*, 12129–12137.
- (61) Becke, A. D. A New Mixing of Hartree–Fock and Local Density-functional Theories. *J. Chem. Phys.* **1993**, *98*, 1372–1377.
- (62) Weigend, F.; Ahlrichs, R. Balanced Basis Sets of Split Valence, Triple Zeta Valence and Quadruple Zeta Valence Quality for H to Rn: Design and Assessment of Accuracy. *Phys. Chem. Chem. Phys.* **2005**, *7*, 3297–3305.
- (63) Jacquemin, D.; Perpète, E. A.; Scuseria, G. E.; Ciofini, I.; Adamo, C. TD-DFT Performance for the Visible Absorption Spectra of Organic Dyes: Conventional versus Long-Range Hybrids. *J. Chem. Theory Comput.* **2008**, *4*, 123–135.
- (64) Senevirathna, W.; Liao, J.-y.; Mao, Z.; Gu, J.; Porter, M.; Wang, C.; Fernando, R.; Sauvé, G. Synthesis, Characterization and Photovoltaic Properties of Azadipyrromethene-Based Acceptors: Effect of Pyrrolic Substituents. *J. Mater. Chem. A.* **2015**, *3*, 4203–4214.
- (65) Jimenez, J. C.; Zhou, Z.; Rheingold, A. L.; Parker, S. M.; Sauvé, G. Tuning the Properties of Azadipyrromethene-Based Near-Infrared Dyes Using Intramolecular BO Chelation and Peripheral Substitutions. *Inorg. Chem.* **2021**, *60*, 13320–13331.
- (66) Franzke, Y. J.; Holzer, C.; Mack, F. NMR Coupling Constants Based on the Bethe–Salpeter Equation in the GW Approximation. *J. Chem. Theory Comput.* **2022**, *18*, 1030–1045.
- (67) Grimme, S. Stda Program for Computing Excited States and Response Functions via Simplified TD-DFT Methods (sTDA, sTD-DFT, and SF-sTD-DFT). 2022; <https://github.com/grimme-lab/stda>.
- (68) Clark, A. E.; Davidson, E. R. Population Analyses That Utilize Projection Operators. *International Journal of Quantum Chemistry* **2003**, *93*, 384–394.
- (69) Bruhn, G.; Davidson, E. R.; Mayer, I.; Clark, A. E. Löwdin population analysis with and without rotational invariance. *International Journal of Quantum Chemistry* **2006**, *106*, 2065–2072.
- (70) Zhou, Z.; Parker, S. M. Accelerating Molecular Property Calculations with Semiempirical Preconditioning. *J. Chem. Phys.* **2021**, *155*, 204111.
- (71) Domínguez, A.; Aradi, B.; Frauenheim, T.; Lutsker, V.; Niehaus, T. A. Extensions of the Time-Dependent Density Functional Based Tight-Binding Approach. *J. Chem. Theory Comput.* **2013**, *9*, 4901–4914.
- (72) Eichkorn, K.; Weigend, F.; Treutler, O.; Ahlrichs, R. Auxiliary basis sets for main row atoms and transition metals and their use to approximate Coulomb potentials. *Theor. Chem. Acc.* **1997**, *97*, 119.
- (73) Tao, J.; Perdew, J. P.; Staroverov, V. N.; Scuseria, G. E. Climbing the Density

Functional Ladder: Nonempirical Meta-Generalized Gradient Approximation Designed for Molecules and Solids. *Phys. Rev. Lett.* **2003**, *91*, 146401.

- (74) Grimme, S.; Antony, J.; Ehrlich, S.; Krieg, H. A Consistent and Accurate Ab Initio Parametrization of Density Functional Dispersion Correction (DFT-D) for the 94 Elements H-Pu. *J. Chem. Phys.* **2010**, *132*, 154104.
- (75) Grimme, S.; Ehrlich, S.; Goerigk, L. Effect of the Damping Function in Dispersion Corrected Density Functional Theory. *J. Comput. Chem.* **2011**, *32*, 1456–1465.
- (76) Zhou, Z. escfrisprep: a plugin for the TDDFT-ris and TDDFT-ris+p method in TURBOMOLE, Github. 2022; <https://github.com/John-zzh/TDDFT-ris>.
- (77) Zhou, Z.; Della Sala, F.; Parker, S. M. Minimal auxiliary basis set approach for the electronic excitation spectra of organic molecules, OSF, Dataset. 2022; <https://osf.io/x5bsv>.